Microscopy and spectroscopy on model catalysts in gas environments

Wenzel, S.

Chapter 3

Stability of ZnO($10\bar{1}0$) in Moderate Pressures of Water

3.1 Introduction

Global warming and the depletion of natural resources are among the greatest and most urgent challenges humankind is currently facing. There is an obvious need for alternative methods of transportation and energy production. Renewable energy sources like wind and solar power however are time and weather dependent and thus require simultaneous advances in energy-storage techniques. Methanol is interesting as an energy-storage material. It can be produced from renewable sources [69], is biodegradable [70], and, being liquid at room temperature [71], it can be stored more easily and safely than hydrogen. In order to harvest the energy, methanol can be converted to hydrogen via the methanol steam reforming reaction:

$$CH_3OH + H_2O \rightarrow 3\ H_2 + CO_2 \tag{3.1}$$

Advantages of methanol with respect to other reforming feedstocks are the high H-to-C ratio and a reaction temperature as low as 250 °C [72]. Carbon monoxide forms as a side product to the methanol steam reforming reaction [73]. This is the main challenge in converting the hydrogen further to electricity using a fuel cell. The platinum anode of fuel cells is poisoned by a few parts per million of CO [74]. The requirement for a viable methanol steam reforming catalyst is thus a high selectivity towards CO_2 instead of CO. The industrially used catalyst for methanol synthesis Cu-ZnO/Al_2O_3 shows significant activity for methanol steam reforming and has been researched extensively [72,75,76]. Although there is ample evidence regarding the nature of strong metal-support interactions between copper and zinc oxide [72,77,78], the exact mechanism of the methanol steam reforming remains under debate.
Zinc oxide alone is active itself and relevant for the CO_2 selectivity of the methanol steam reforming catalyst [79,80]. Studies on zinc oxide single crystals of different faces are aiming at understanding its role at the atomic level. The interaction of ZnO(10$\bar{1}$0) with methanol [81–83], water [84,85], atomic hydrogen [86], CO [87,88], and CO_2 [89,90] has been studied extensively under ultra-high vacuum conditions. Among these studies are microscopy measurements as well as diffraction, desorption spectroscopy, and theoretical studies. Spectroscopy measurements on the interaction with water have been conducted under near-ambient pressure conditions [91]. However, to our knowledge, there is no microscopy study showing the surface under these conditions. The ReactorSTM setup [44] allows for combining controlled ultra-high vacuum preparation with nanometer-scale imaging in the mbar range of water. In the following we characterize the ZnO(10$\bar{1}$0) surface in ultra-high vacuum (Section 3.3.1) and present ex situ as well as in situ imaging of ZnO(10$\bar{1}$0) in moderate pressures of water (Sections 3.3.2 and 3.3.4), investigate the role of surface hydroxylation (Section 3.3.3) and give preliminary results on the influence of a hydrogen environment (Section 3.3.5).

3.2 Materials and Methods

3.2.1 The ReactorSTM

The experimental setup has been described in detail by Herbschleb et al. [44]. In short, the scanning tunneling microscope (STM) can be used in ultra-high vacuum (base pressure $< 10^{-9}$ mbar) as well as in up to 6 bar of gases. This is possible in a flow reactor cell of about 0.05 ml volume, which is closed off from the rest of the vacuum chamber by the sample, the STM body, and a Kalrez seal. The video-rate control electronics were described by Rost et al. [92] and the control software is Camera 6.1. [93]. A cut platinum iridium wire (Pt90/Ir10, 0.25 mm) is used for the STM tip. During a scan on a cleaned Au(111) single crystal the tip can be prepared by tip pulsing and the distance and height are calibrated. The STM images are processed in WSxM [94].
Complementary techniques available in the same setup are a low-energy electron diffraction (LEED) and Auger electron spectroscopy (AES) system with 4-grid analyzer (Omicron SpectaLEED with NG LEED S control unit and DATAuger software) and X-ray photoelectron spectroscopy (XPS) with a VG Microtech dual anode X-ray source and a Clam 2 analyzer. For the use of these techniques the ReactorSTM setup consists of multiple chambers with different measurement stations and the sample is fixed to a holder which can be moved between them while staying in UHV. The holder allows for heating with a filament behind the sample as well as e-beam heating induced by a positive voltage directly on the sample. To enable this e-beam heating for oxide samples and to protect them from uneven heating from the filament a metal plate is placed underneath the sample. It is electrically connected to a ring-shaped plate holding the crystal from the top. Tungsten was chosen for sufficient heat conductivity of these plates [95]. They are directly connected to the high voltage connection. Additionally, this connection functions as the ground connection during argon sputtering, LEED/Auger, and X-ray photoelectron spectroscopy, as well as the bias voltage connection for scanning tunneling microscopy. A K-type thermocouple consisting of two 0.125 mm thick wires is spot-welded to the top plate. The temperature read-out for oxide samples is made as accurate as possible by heating up and cooling down slowly (at maximum 1 K/s). Additionally, this ensures that the crystal is not damaged due to uneven heating. In general it has to be noted that the temperature read-out in the ReactorSTM setup has an off-set due to junctions of other materials within the thermocouple connections, which are needed for technical reasons. The off-set of the temperature read-out was thoroughly investigated in [96] and leads to an underestimation of the annealing temperature used for zinc oxide in this thesis by about 120 K.
The ZnO($10\bar{1}0$) single crystal was purchased from SPL.

3.2.2 Water Content of Gases in the ReactorSTM

The reactor volume inside the ReactorSTM can be filled with up to 6 bar of gases via capillaries originating from a dedicated gas mixing system, which is built in-house. Downstream of the reactor the gases can be analyzed using a quadrupole mass spectrometer (Stanford Research Systems RGA100). For this purpose a Vacgen LVM series leak valve is adjusted in-house in order to leak a part of the line content into a separate UHV chamber (base pressure 5×10^{-9} mbar) where the mass spectrometer is located. The gases used here are argon 5.0 from Westfalen [97] and hydrogen 5.0 from Air Liquide [98], both with a water content below 3 volume parts per million. In order to determine the amount of water that reaches the sample, the gas line was filled with 1 bar of argon or hydrogen, respectively, with a leak of 10^{-6} mbar into the mass spectrometer chamber in order to measure the argon, hydrogen, and water signals. The measured backgrounds in the spectrometer chamber (with the leak valve closed) are subtracted from the measurements. Relative sensitivity factors for ionization and fractioning are approximated using Ref. [99]. This results in a measured ratio of water-to-argon partial pressure of $(5.0 \pm 0.3) \times 10^{-3}$ in 1 bar argon and water-to-hydrogen partial pressure of $(2.7 \pm 0.3) \times 10^{-3}$ in 1 bar hydrogen. The error of $\pm\, 0.3 \times 10^{-3}$ was estimated by repeating the same argon measurement multiple times and with different argon flows. A source of systematic overestimation of the amount of water could be that the leak rate through the leak valve increases with increasing mass [100]. However, this difference is likely not larger than one order of magnitude. Thus, we estimate the amount of water in 1 bar of argon or hydrogen to be on the order of 1 mbar. As this is orders of magnitude above the amount that is contained in the gas bottles, the majority of the water must originate from other parts of the gas line and the amount will be roughly the same for all gases used in this experimental setup. Although the majority of the gas lines are flushed with inert gas and heated to at least 90 °C before every use of the gas supply system, some parts cannot be cleaned in this manner. First, the temperature in areas with sensitive electronic equipment such as mass flow controllers cannot surpass 65 °C. Second, the high-pressure parts of the gas lines right after the gas bottles (up to 200 bar) cannot be heated and flushed properly as the gas flow is limited to the 10 ml/min range by the mass flow controllers. This could be improved in the future by installing additional connections between these high-pressure parts and the pump such that they can be flushed repeatedly with a high flow. Due to the requirements for mechanical stability and pressure stability for the in situ STM setup a cold trap to reduce the water content reaching the reactor is not suited. The installation of catalytic water traps into the existing gas system has not been successful so far.

3.2.3 XPS Fitting

The X-ray photoelectron O 1s peaks were fitted using CasaXPS 2.3.19. A zinc Auger peak with a tail towards high binding energies partly overlaps with the oxygen peak such that the background on its low binding-energy side appears too high and higher than on the high binding-energy side. The widely used Shirley background subtraction models the influence of inelastically scattered photoelectrons, which leads to a background that is higher on the high binding-energy side instead. Thus, a Shirley background is not appropriate here and a linear background was chosen. As the background on the low binding-energy side is overestimated, the O 1s peak stemming from the ZnO itself, which we will refer to as the bulk oxygen peak, is likely underestimated in comparison to any other O 1s peaks which are shifted to higher binding energies. We identify a peak at + 1.5 eV with respect to the bulk peak as adsorbed OH and a peak with a shift of + 3.5 eV as molecularly adsorbed water on top of the hydroxylated surface [101]. The shifts of these peaks were fixed during fitting and the full width half maximum of all peaks was constrained. As the bulk O 1s peak shows a larger full width half maximum than the Zn $2p_{3/2}$ peak, the width is not determined by instrumental parameters, but mainly by the chemical states. Therefore, the constraint for the OH and H_2O peaks was chosen larger (maximally 3.5 eV) than the constraint for the bulk peak (maximally 3 eV). Gaussian-Lorentzian product functions with a ratio of 1:1 gave the most satisfactory fit.

Following the procedure described in Ref. [86] the bulk oxygen peak was fixed to 530.4 eV in order to compensate for overall shifts of the measured binding energy. The result is in agreement with calibration of the energy using the Zn $2p_{3/2}$ peak or the Au 4f peak of a Au(111) single crystal to within 0.5 eV. Significant charging of the ZnO can thus be excluded.

The relative peak areas of the OH and the H_2O peaks, A_{OH}/A_{total} and A_{H_2O}/A_{total} respectively, with $A_{total} = A_{bulk} + A_{OH} + A_{H_2O}$, are used as a measure for the amount of hydroxylation and adsorbed molecular water. Additionally, they can be compared to an estimation of the relative peak area for one monolayer according to the Lambert-Beer absorption law approximation [101,102]. We are using $(A_{OH}/A_{total})|_{1ML} = 1 - \exp(-t/\lambda)$ with the thickness of one monolayer of t = 0.26 nm [91] and the inelastic mean free path of λ = 1.9 nm estimated using the TPP-2M formula in the NIST database [103] for an electron kinetic energy of 957 eV, which corresponds to the O 1s binding energy of 530 eV probed using an X-ray energy of 1487 eV (aluminum K_α).

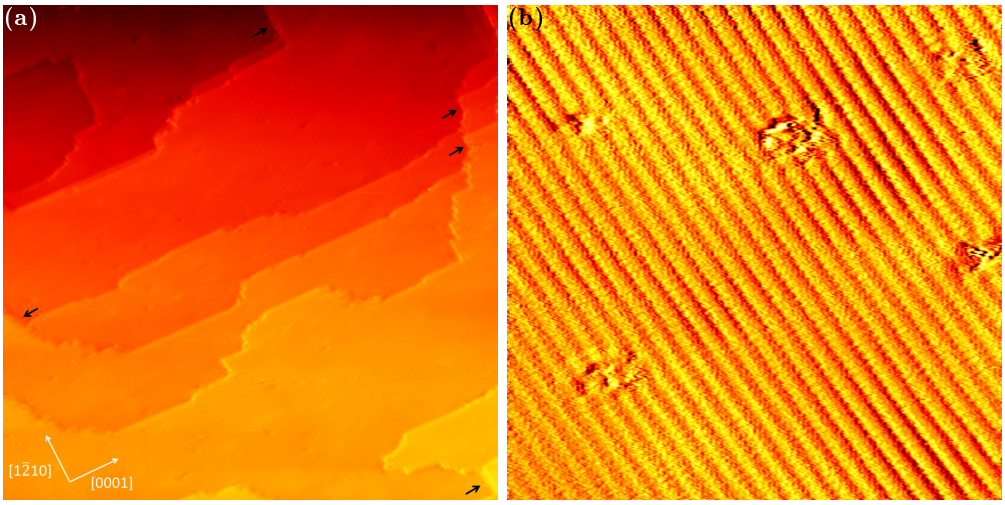

Figure 3.1: (a) 80 nm x 80 nm STM image of the as-prepared ZnO(10$\bar{1}$0) surface taken at 400 K with + 3 V and 50 pA. The plane filter image was merged with its derivative. Black arrows mark double steps parallel to the [1$\bar{2}$10] direction. (b) 17 nm x 17 nm STM image of the same surface taken at 400 K with + 2.5 V and 50 pA. The plane filter image was merged with its derivative in a ratio of 2:1.

3.3 Results and Discussion

3.3.1 As-prepared ZnO(10$\bar{1}$0) in UHV

The ZnO(10$\bar{1}$0) surface was prepared by cycles of 20 min sputtering in $1{\cdot}10^{-6}$ mbar of argon with an acceleration voltage of 1.4 kV resulting in a sample current of 4 μA on a surface area of 0.5 cm^2 followed by 20 min of annealing to 795 K in ultra-high vacuum. More details about the preparation and imaging in UHV can be found in the supplemental information (Section 3.5.1). Figure 3.1 shows the ZnO(10$\bar{1}$0) surface at 400 K after about 100 of these cleaning cycles. 10-nm to 40-nm-wide flat terraces are visible in the large-scale image in (a) with two types of step edges orthogonal to each other. The step heights in this image measure as (0.30 $\pm$ 0.04) nm which is in agreement with the value of 0.281 nm expected from the crystal structure [104]. In the smaller-scale image in Figure 3.1(b) regular parallel lines are visible. Their distance, averaged over measurements on multiple images, is (0.59 $\pm$ 0.09) nm, which can be identified as the size of the unit cell in the [0001] direction by comparison to the value of 0.521 nm based on the crystal structure. A schematic of the ZnO(10$\bar{1}$0) surface can be found in the supplemental information (Figure 3.15). The higher lines can be attributed to the Zn surface atoms [105] whereas the oxygen atoms in between appear lower in STM. On

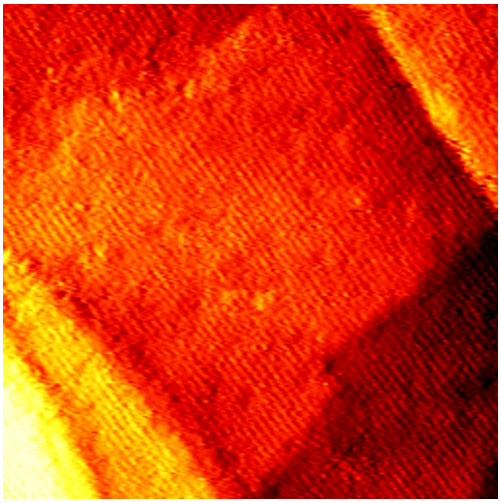

Figure 3.2: 40 nm x 40 nm STM image of the as-prepared ZnO($10\bar{1}0$) surface taken at room temperature with + 4 V and 50 pA. The plane filter image was merged with its derivative for better visibility of the Zn lines.

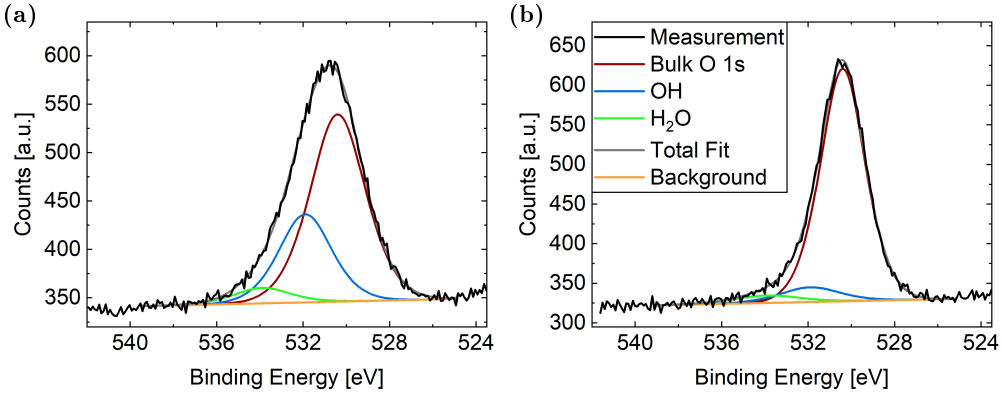

Figure 3.3: O 1s spectra of the as-prepared ZnO($10\bar{1}0$) taken at (a) 300 K and (b) 400 K. A linear background was subtracted and the fitted peaks are Gaussian-Lorentzian product functions with a ratio of 1:1. The details of the fitting procedure are described in the Materials and Methods Section 3.2.3.

the basis of the lines of Zn atoms, the orientation of the sample can be identified as indicated by the arrows overlaid on the image in Figure 3.1(a). The Zn lines in Figure 3.1(b) are interrupted in five positions, which can be identified as surface vacancies. These are investigated in more detail in the supplemental information (Section 3.5.2). The larger-scale color variations in this image are likely due to the incorporation of argon, see the supplemental information (Section 3.5.3).

At room temperature the resolution on ZnO(10$\bar{1}$0) is generally lower than at 400 K in our scanning tunneling microscope. However, the Zn lines can still be visible as shown in Figure 3.2. Figure 3.3 is a comparison between the O 1s X-ray photoelectron peaks at room temperature and 400 K. The fitting procedure is explained in Section 3.2.3. Apart from the O 1s peak of bulk ZnO at 530.4 eV [106], two additional peaks, adsorbed OH and H_2O, are necessary for a satisfactory fit. In the following we use the ratio of the areas underneath the OH and H_2O peaks with the total O 1s peak as a measure for the amount of hydroxylation and molecularly adsorbed water, respectively. For the OH peak these relative areas are 0.29 at room temperature and 0.07 at 400 K, whereas the relative area of the H_2O peak is 0.05 at room temperature and 0.04 at 400 K. The amount of hydroxylation at 400 K is thus only 24 % of the amount of hydroxylation at 300 K. Heinhold et al. measure the relative OH area to decrease to roughly 70 % when increasing the temperature from 300 K to 400 K (estimated from Figure 4.(a) in Ref. [101]). Their coverage only falls below a monolayer above roughly 670 K. Using the same Lambert-Beer law approximation (see Section 3.2.3) a monolayer of OH would correspond to a relative OH peak area of 0.13 here. This estimates the coverage at 400 K to be about 50 % of a monolayer. The discrepancies between the measurements done here and the results of Heinhold et al. could stem from the difference in preparation method of the ZnO(10$\bar{1}$0) surface. A more comparable preparation method was used by Newberg et al. [91]. Near-ambient pressure XPS allowed for their measurements in a significantly higher pressure regime on the order of 10^{-1} mbar of water. Although the surface is saturated with OH below 550 K under these conditions, no molecularly adsorbed water was observed in their measurements. In general, discrepancies between the measurement done here and other literature could stem from a partly overlapping Zn Auger peak with the O 1s peak, which, as described in Section 3.2.3, leads to an underestimation of the bulk ZnO oxygen peak and thus an overestimation of the OH and H_2O relative peak areas. This could explain why a relative OH peak area significantly above the value estimated for one full monolayer was measured for 300 K, although one monolayer is identified as the saturation coverage in Ref. [91]. Thus, no accurate coverage values can be given here. However, the photoelectron spectroscopy measurements have shown that more (partly dissociated) water is present on the surface at 300 K in comparison to 400 K.

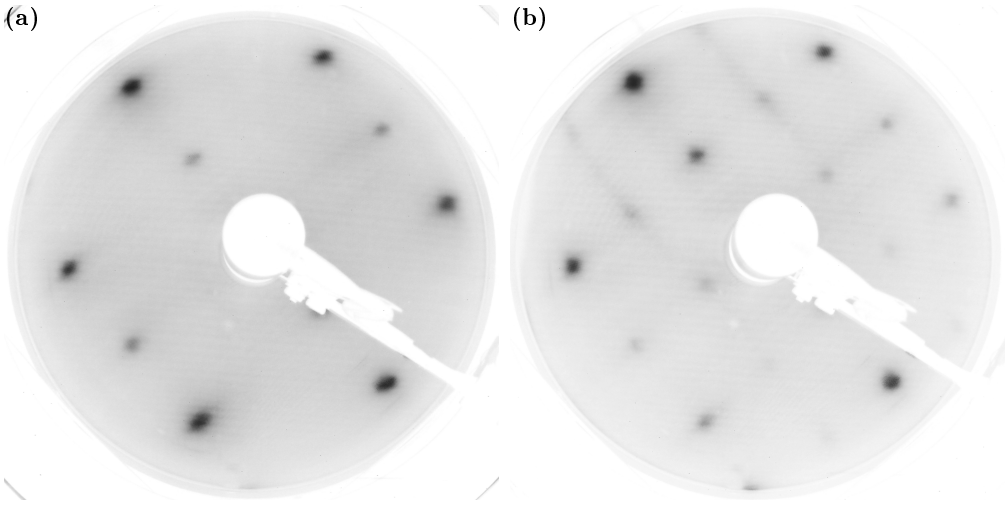

Figure 3.4: Low-energy electron diffraction pattern of ZnO($10\bar{1}0$) at (a) 400 K compared to (b) room temperature taken at 52.1 eV electron energy.

The first water layer on ZnO($10\bar{1}0$) can be mobile and locally switch between a molecular and a half-dissociated layer as observed with scanning tunneling microscopy by Dulub et al. [84]. This can account for the more challenging scanning observed here at room temperature in comparison to 400 K despite the ability of water to increase the conductivity of ZnO [107]. However, the areas of the H_2O and OH peaks in XPS at room temperature do not show the same amount of molecularly adsorbed water and dissociated water but merely 18 % as much H_2O as OH. Following Ref. [101] it can be argued that the water molecules in the first adsorption layer, which adsorb with their oxygen atom on the zinc surface atoms, do have strong hydrogen bonds with the neighboring surface oxygen atom, also in the case that this does not lead to dissociation. Therefore, the non-dissociated water in the first layer might rather contribute to the OH peak than the H_2O peak and it is not possible to distinguish between the molecularly adsorbed and the half-dissociated first layer using XPS. However, the half-dissociated layer can be seen in low-energy electron diffraction. Figure 3.4 shows the comparison of low-energy electron diffraction patterns on the ZnO($10\bar{1}0$) surface at room temperature and 400 K, respectively. Whereas the same rectangular unit cell of the substrate is visible in both patters, the room temperature LEED shows an additional 2x1 overlayer. This confirms the presence of the half-dissociated layer, which has been calculated to be the most stable structure in ultra-high vacuum [108,109].

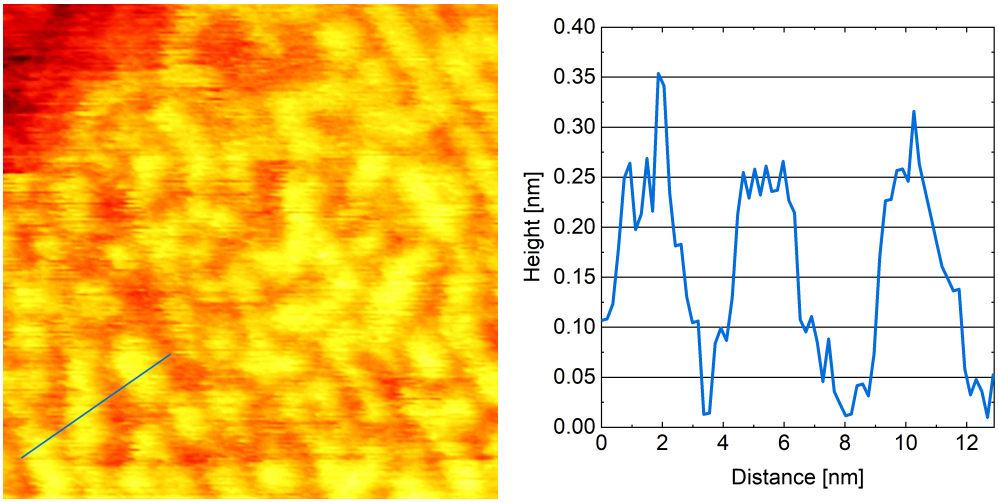

Figure 3.5: 35 nm x 35 nm STM image of ZnO(10$\bar{1}$0) after 10 min in roughly 1 mbar of water at room temperature with the corresponding height profile. The image is taken in UHV at room temperature with + 3 V and 50 pA. Including the initial filling of the reactor up to 1 bar of argon carrier gas the total exposure to the water flow is roughly 19 min (see experiment II in Figure 3.9).

3.3.2 Rough Phase of ZnO(10$\bar{1}$0)

Figure 3.5 and the larger-scale overview in Figure 3.6 show the ZnO(10$\bar{1}$0) surface after exposure to roughly 1 mbar of water for 10 min. The corresponding height profile on the right side of Figure 3.5 shows a height difference between the terrace and the newly formed structure of between 0.23 nm and 0.33 nm. Although the accuracy of this value is limited by the ability of the tip to follow the rapid height changes, the measured height difference is in agreement with the step height of ZnO(10$\bar{1}$0) suggesting that the surface has roughened. This is confirmed by the stability of this phase in ultra-high vacuum for several days as well as the ability of the surface to flatten out again when annealing, as shown in Figure 3.7. After 10 min annealing at 795 K there is some local roughness left, which does however not cover the whole terrace anymore. At the same time medium-sized holes, one step height lower than the original terraces, appear, which are evidence of the rearrangement taking place during annealing. These holes are still present after a total of 20 min annealing and even larger ones exist as they merge during the rearrangement. The local roughness is gone completely after 20 min of annealing. In order to remove all medium-sized holes and restore the flatness of the as-prepared sample (see Figure 3.1(a)) annealing for a total of 2 hours is necessary.
The overview image of the rough surface in Figure 3.6 allows for an estimation of the

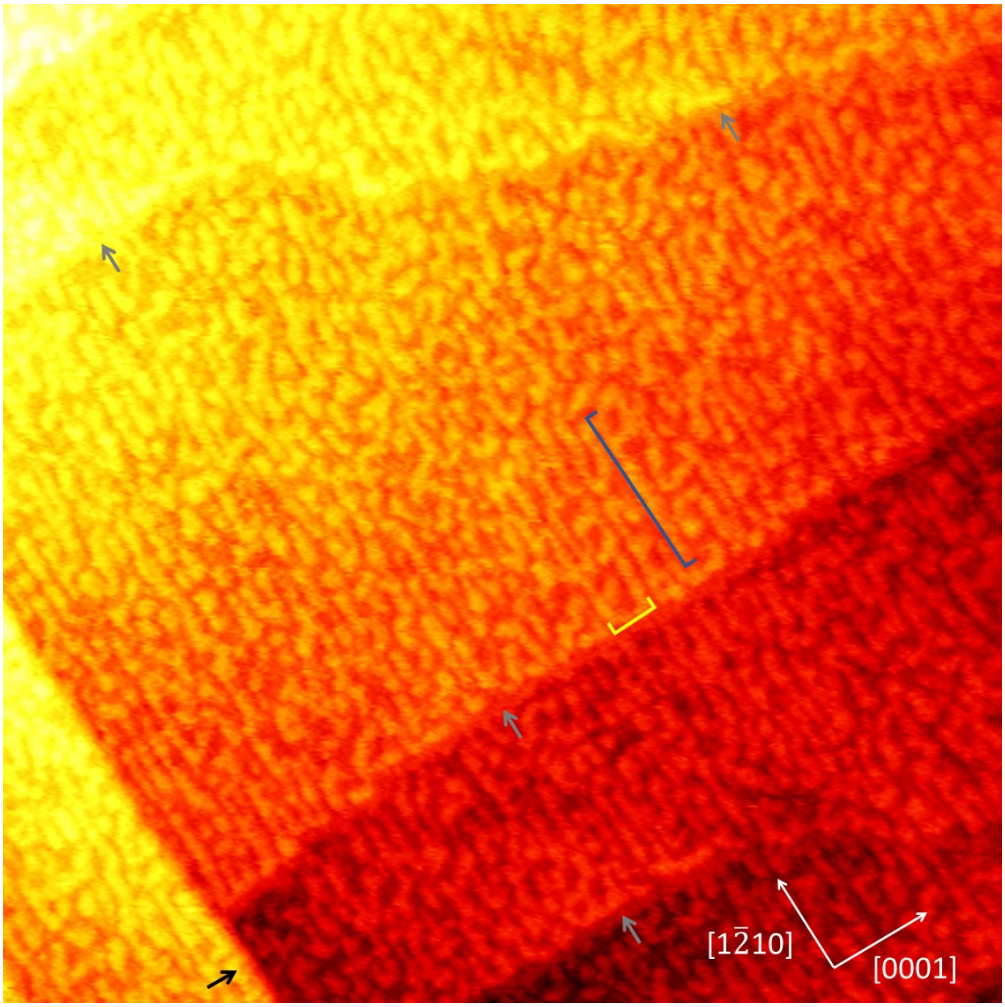

Figure 3.6: 150 nm x 150 nm STM image of ZnO(10$\bar{1}$0) after 10 min in 1 mbar of water at room temperature. The image is taken in UHV at room temperature with + 3 V and 50 pA. For better visibility of the steps as well as the structure on the terraces the plane filter image was merged with its derivative at a ratio of 2:1. Examples of areas with the same height are marked with a blue line parallel to the [1$\bar{2}$10] direction and a yellow line parallel to the [0001] direction. A black arrow marks a (000$\bar{1}$)-type double step. Grey arrows mark (1$\bar{2}$10)-type steps accompanied by a 2-nm-wide area without height differences.

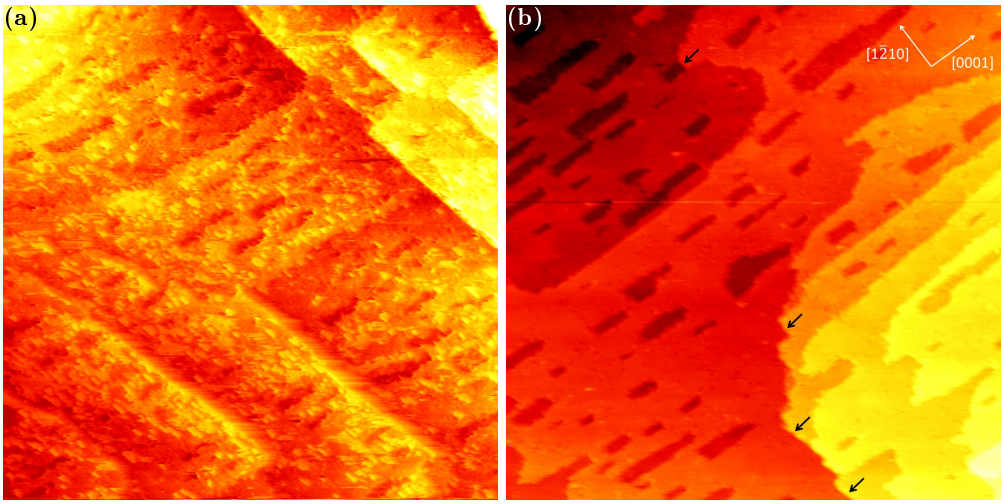

Figure 3.7: 150 nm x 150 nm STM images of ZnO(10$\bar{1}$0) after 10 min in 1 mbar of water at room temperature and subsequent annealing at 795 K for (a) 10 min and (b) 20 min. The images were taken at 400 K with + 3 V and 50 pA. Although step edges are clearly visible by eye in (a), the different terraces could not be properly identified using the local plane filter in WSxM. This could be due to the inhomogeneity on the terraces. For better visibility of the remaining small-scale roughness the image was merged with its derivative at a ratio of 2:1. Black arrows in (b) mark double steps parallel to the [1$\bar{2}$10] direction.

typical size of areas with the same height. In the [0001] direction the size is between 2 and 4 nm with some longer areas up to 7 nm mostly near the step edges. An example is marked with a yellow line. In the [1$\bar{2}$10] direction, however, the areas with the same height are up to 26 nm long. An example is marked with a blue line. This suggests that there is a clear favor for the formation of (0001)- or (000$\bar{1}$)-type steps, which are parallel to the [1$\bar{2}$10] direction, in comparison to the formation of (1$\bar{2}$10)-type steps, which are orthogonal to the [1$\bar{2}$10] direction. The original (1$\bar{2}$10)-type step edges in Figure 3.6 show a roughly 2-nm-wide area without height difference as indicated by the grey arrows. This suggests that, although a large part of the terraces is elevated by one step height, double steps of this type are unfavored. On as-prepared surfaces with a large step density double steps of both types are present (see for example Figure 1(a) in Ref. [110] and Figure 1(a) in Ref. [105]). However, on surfaces with lower step density we have observed more double steps in the parallel direction than the (1$\bar{2}$10) type. Examples of these double steps are marked with black arrows in Figures 3.1(a), 3.6, and 3.7(b). The (1$\bar{2}$10)-type steps and double steps being unfavored suggests a lower stability of the (1$\bar{2}$10) face compared to the (0001) or (000$\bar{1}$) faces of ZnO. Although theory [111] suggests the opposite, (1$\bar{2}$10) is the least stable of the low-index

faces according to experimental data [112]. This is confirmed by STM measurements showing that the $(1\bar{2}10)$-type step edge is the most active site for nucleation during the deposition of Cu on ZnO$(10\bar{1}0)$ [110].
Although the probability of formation of the two different types of steps and double steps during the roughening process in water can be motivated by the stability of the corresponding face, the total ratio of the two different types of single steps on the as-prepared surface does not agree with this difference in stability. The ratio of step types varies significantly with scanning position and in comparison to different publications as it additionally depends on other factors like the preparation procedure and initial miscut of the single crystal.

3.3.3 Hydroxylation and Adsorbed Water

Table 3.1: Relative OH peak areas for different exposure times, flows of water, and exposure temperatures in comparison to the as-prepared sample (in the first column) including XPS measurements taken at 400 K as well as at 300 K.

Exposure Time [min]	-	10	10	10	240
Flow [ml/min]	-	1	2	1	1
Exposure Temperature [K]	-	300	300	400	400
Relative OH peak area at 400 K	0.07	0.04	0.12	0.08	0.06
Relative OH peak area at 300 K	0.29	0.12	0.18	0.12	0.15

Table 3.2: Relative H_2O peak areas for different exposure times, flows of water, and exposure temperatures in comparison to the as-prepared sample (in the first column) including XPS measurements taken at 400 K as well as at 300 K.

Exposure Time [min]	-	10	10	10	240
Flow [ml/min]	-	1	2	1	1
Exposure Temperature [K]	-	300	300	400	400
Relative H_2O peak area at 400 K	0.04	0.1	0.12	0.16	0.14
Relative H_2O peak area at 300 K	0.05	0.08	0.09	0.13	0.09

X-ray photoelectron spectroscopy measurements of the O 1s peak have been taken after exposure to argon. As explained in the supplemental information (Section 3.5.4), the ZnO$(10\bar{1}0)$ surface has to be heated to 400 K in order to remove it from the reactor. Therefore, every XPS measurement was first done at this temperature and once more after cooling down to 300 K. The relative areas of the OH as well as H_2O

peaks, calculated as described in Section 3.2.3, are used as a measure for the amount of hydroxylation and molecularly adsorbed water, respectively. By comparing multiple measurements taken after the same exposure (data not shown) the accuracy of the relative peak areas can be roughly estimated as $\pm$ 0.05. This value is taken into account in the following when interpreting the relative peak areas presented in Tables 3.1 and 3.2 for different exposures. Comparing all values taken at 400 K to the as-prepared surface at 400 K, the exposure does not increase the hydroxylation to a detectable amount. Letting the surface cool down to 300 K, the amount of hydroxylation increases for every measurement, however it does not reach the level measured on the clean sample at 300 K. This could be due to a longer waiting time before taking the XPS spectra on the clean sample, which indicates that the hydroxylation increases over time in UHV. An increase in the H_2O relative peak area is detected right after the exposure in the measurements taken at 400 K compared to the clean sample at the same temperature. A part of this molecularly adsorbed water has desorbed when the XPS is measured at 300 K as can be seen in a decrease in the relative peak areas for all measurements. As the desorption of water cannot be caused by the decrease in temperature, this effect can only be attributed to the longer time passed since the end of the exposure. Given the accuracy of the relative peak areas of $\pm$ 0.05 the values measured at 300 K after exposure are comparable with the as-prepared surface. Thus, the desorption of the molecularly adsorbed water after the exposure proceeds faster than the increase of hydroxylation in UHV.
As the rough phase is stable in UHV at 300 K as well as 400 K, it can be concluded that, although the formation is induced by water, the presence of the rough phase is not directly correlated to the amount of hydroxylation and molecularly adsorbed water left on the surface after the end of the water exposure. This is additional evidence that the rough phase consists of zinc and oxygen atoms from the surface itself.

3.3.4 Roughening Process

Figure 3.8 shows the structural change of ZnO(10$\bar{1}$0) in 1 bar of argon containing roughly 1 mbar of water. (A quantification of the water content is presented in Section 3.2.2.) The roughening process starts at multiple positions on the terrace and the surface is completely roughened 7.4 min afterwards. In comparison to the ex situ image in Figure 3.5, the in situ images presented here show horizontal streaks and the shapes can be distorted. In general, the presence of gas can disturb the tunneling electrons. Sample drift under the high pressure as well as the clear mobility of surface atoms during the structural change further disturb the imaging in this case.
Figure 3.9 compares two different measurements of the formation of the rough phase where different flows of carrier gas were used. Colored areas indicate the time from the

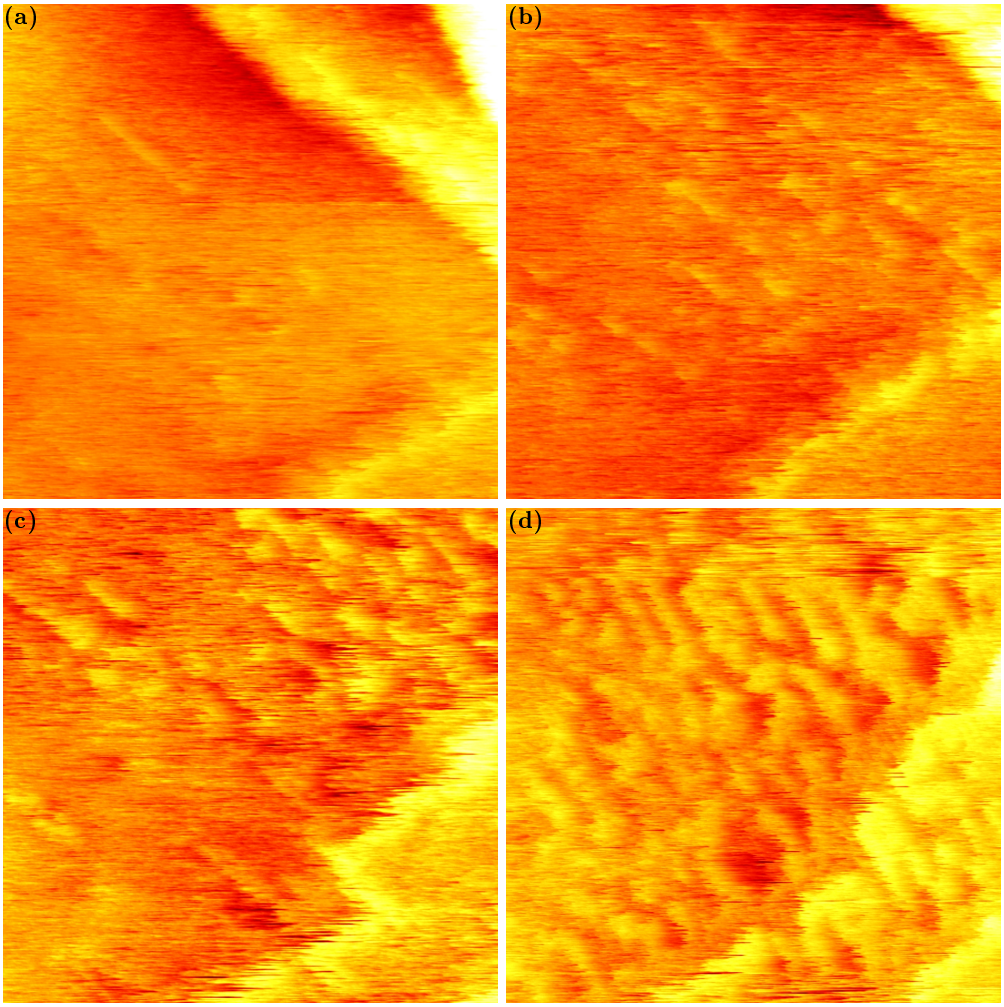

Figure 3.8: 35 nm x 35 nm STM images of ZnO($10\bar{1}0$) in roughly 1 mbar of water at room temperature taken with + 2 V and 50 pA. The images were taken (a) 13.0 min, (b) 14.2 min, (c) 16.7 min, and (d) 20.4 min after starting the flow of gas.

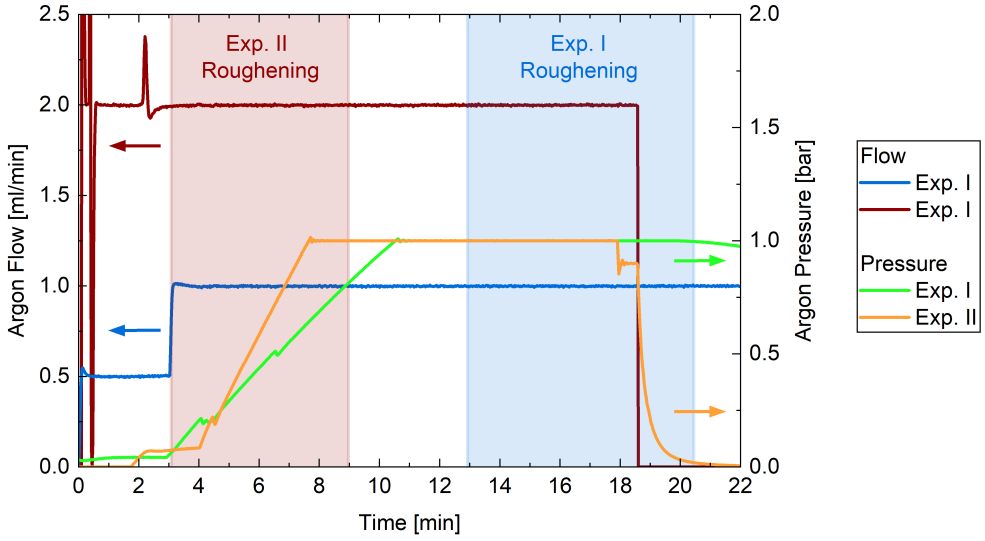

Figure 3.9: Flow and pressure curves of two different exposures to up to 1 bar of wet argon. The colored areas indicate the roughening of the ZnO(10$\bar{1}$0) as observed in STM. Experiment I corresponds to the STM images shown in Figure 3.8. The higher peaks seen at the beginning of the flow are caused by a pressure build-up that is released when opening the mass flow controller. Another peak in the flow of experiment II after 2 min is likely due to a necessary adjustment of the argon pressure in the gas line leading to the mass flow controller.

moment where the roughening can first be seen, like in Figure 3.8(a), until the point where the terraces are fully roughened, like in Figure 3.8(d). With an argon flow of up to 1 ml/min (experiment I) the roughening only starts when 1 bar has been reached after 13 min of flow and a total of 11 ml of gas passing by the sample. In contrast, when an argon flow of 2 ml/min is used (experiment II), the roughening starts significantly earlier, at 0.075 bar after 3 min of flow and a total of 6 ml of gas passing by the sample. This total amount of gas is likely underestimated in experiment II due to the initial high flow peaks before stabilizing to the desired flow as seen in Figure 3.9. Additionally, the scanning velocity in these measurements was chosen such that each STM image takes slightly more than one minute. This limits the accuracy in determining when the roughening starts and when it fills the whole terrace, respectively, and thus for the total amounts of flown gas calculated here. Still the clearly faster onset of formation with larger flow even at a significantly lower pressure suggests that the water pressure is not the main factor that allows for the roughening of the surface to begin and a pressure of less than 1 mbar of water would be sufficient. The time from the onset of roughening until the terrace is fully roughened is shorter as well using the larger flow.

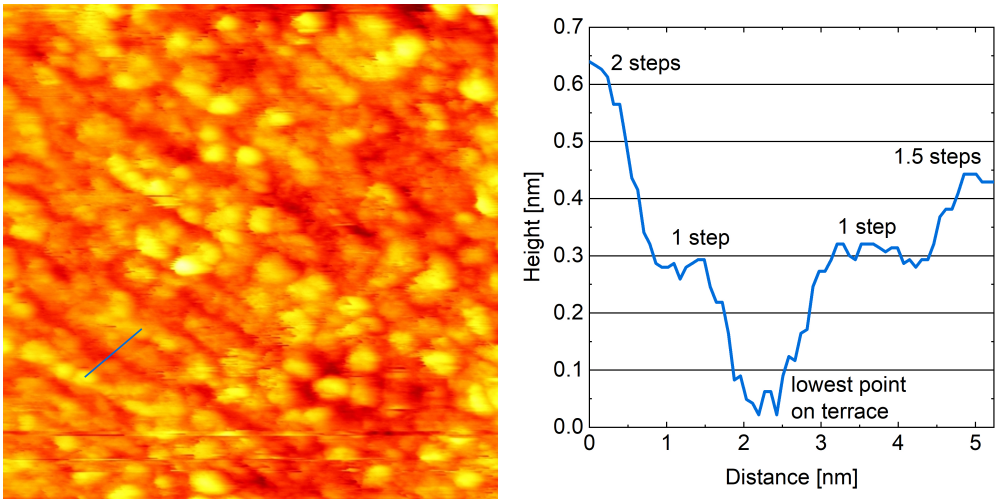

Figure 3.10: 35 nm x 35 nm STM image of ZnO($10\bar{1}0$) after 4 h in 1 mbar of water at 400 K with the corresponding height profile indicated in blue. The image is taken in UHV at room temperature with + 4 V and 50 pA.

In experiment II it takes 5.8 min and a total amount of 11 ml of gas and with the lower flow 7.4 min, but only a total amount of 7.5 ml of gas. Thus, the speed of formation increases less than linearly with the flow. It is possible that, once a sufficient amount of water for the onset of the roughening has been supplied to the surface, the higher pressure in experiment I does lead to a more efficient use of the flown gas.
Under prolonged exposure the ZnO($10\bar{1}0$) roughens more severely. Figure 3.10 shows an STM image after 4 h in roughly 1 mbar of water. (For technical reasons this exposure was done at 400 K surface temperature.) As can be seen in the corresponding height profile, the height difference on one terrace can be twice the step height of ZnO($10\bar{1}0$). Areas with a height difference of about 1.5 times the step height with respect to the lowest point on the terrace are observed as well. As explained in Section 3.5.2, one step consists of two layers of ZnO dimers allowing for the observation of steps with about half the height when the topmost layer is missing. Apart from height differences that correspond to full or half steps, smaller height variations on the small terraces can be seen in Figure 3.10. This suggests that the density of smaller vacancies increases as well. If they for example consist of only one missing dimer, they might not be resolved completely and therefore appear less deep than half the step height. Additionally, the surface could become increasingly amorphous with longer exposure and more severe restructuring. As vacancies can interact more strongly with water [113], the speed of the roughening process could increase over time.
Overall, we thus observe a restructuring of the ZnO($10\bar{1}0$) surface which must stem from

an interaction with water that is significantly different from the interaction that leads to the ordered adsorption structures observed in UHV [84]. Theoretical studies on the interaction of ZnO(10$\bar{1}$0) with water confirm that the 2x1 half-dissociated monolayer (with one dissociated and one molecular water molecule per two ZnO(10$\bar{1}$0) unit cells) is the most stable structure in UHV [109,113,114]. However, the structure changes significantly when adding more water as investigated in detail by Kenmoe et al. [109]. When exactly two monolayers of water are present, they observe a double layer to be the most stable, which does not leave any dangling bonds for adsorption of additional water molecules. Thus, from three monolayers on the structure is significantly different again: One layer, the so-called contact layer, is adsorbed on the surface in an ordered fashion while all additional water molecules are adsorbed in a "liquid-like film", which is more amorphous and can move between a number of different configurations. This picture of the water adsorption suggests that from three monolayers on the structure of the contact layer on the ZnO(10$\bar{1}$0) surface does not change significantly when adding more water. This could account for our observation that the roughening does not primarily depend on the exact pressure in the 0.1 to 1 mbar regime investigated here. The dependence on the gas flow, however, could stem from the amount of water molecules that need to pass through the reactor before at least three monolayers are adsorbed and the contact layer is present. The contact layer differs from the 2x1 monolayer in structure and can contain more water molecules, whereas the ratio of dissociated and non-dissociated molecules is comparable [109,114]. Tocci et al. [114] show that the properties of the contact layer lead to a significant increase in proton exchange to and from the surface in comparison to the 2x1 monolayer. Additionally, proton exchange between the dissociated and non-dissociated water molecules in the first layer, which is not possible in the 2x1 monolayer, occurs frequently in the contact layer. This proton mobility could be responsible for allowing a restructuring of the ZnO(10$\bar{1}$0) surface. A restructuring of the polar (0001) face of ZnO under the influence of water has been observed previously by Önsten et al. [115], showing that water and/or proton mobility can induce mobility of zinc and oxygen atoms or the ZnO dimer. They observe a severe roughening of ZnO(0001) after a deposition of 20 L of water, which is explained as an interaction with hydrogen atoms from dissociated water as hydrogen is known to be able to reconstruct this face of ZnO. However, on the ZnO(10$\bar{1}$0) face, although some vacancies are formed, no severe restructuring due to atomic hydrogen has been reported so far. An ordered 1x1 H overlayer is observed in UHV [105]. Interestingly, before the (0001) surface roughens, the observations of Önsten et al. first show an increase in the size of the (0001) terraces under exposure to smaller amounts of water (up to 5 L). Thus, water itself, without a significant amount of leftover H atoms, might in turn stabilize the (0001) face. This could explain the formation of (0001)-type steps

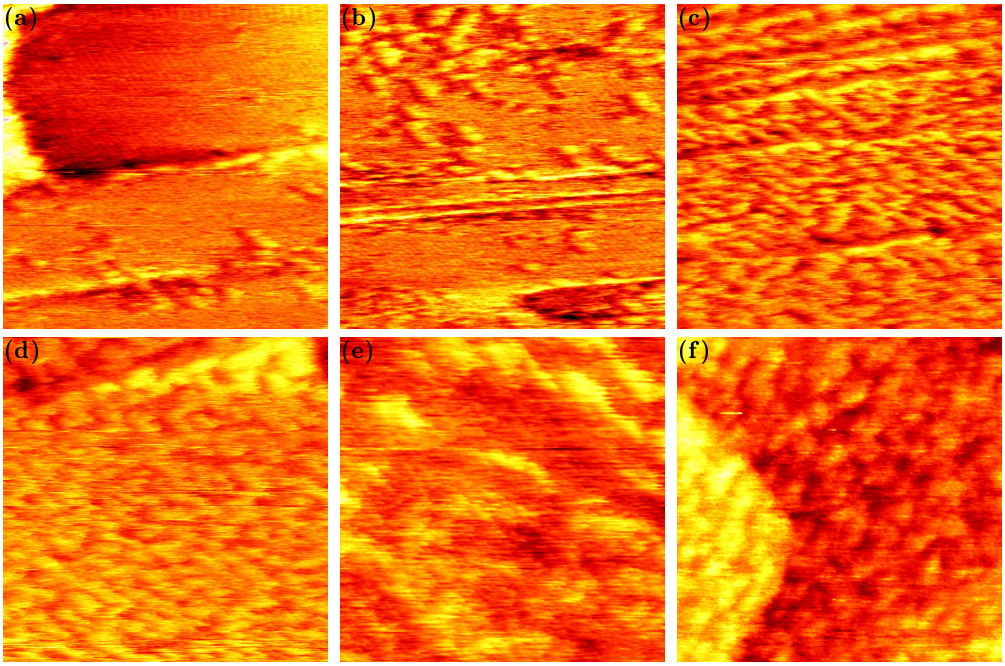

Figure 3.11: 35 nm x 35 nm STM images of ZnO($10\bar{1}0$) in flow of wet hydrogen at room temperature taken after (a) 6.4 min of flow (reactor filled to 0.2 bar), (b) 7.5 min of flow (reactor filled to 0.3 bar), (c) 10.8 min of flow (reactor filled to 0.7 bar), (d) 12 min of flow (reactor filled to 0.8 bar), (e) 20 min of flow (reactor filled to 1 bar), and (f) after the end of the exposure in UHV. The total exposure, consisting of the filling of the reactor as well as 10 min at 1 bar, is 23 min. The images are taken with (a)-(e) + 2.5 V and (f) + 3 V, and 50 pA.

observed here on ZnO($10\bar{1}0$) during the restructuring under the influence of water. As shown in Section 3.3.2, the formation of the (0001)- and ($000\bar{1}$)-type steps is favored over the formation of ($1\bar{2}10$)-type steps. The difference in stability of the different faces and step types, as observed in UHV [110,112], might thus be more severe in moderate pressures of water.

3.3.5 Roughening in Hydrogen Environment

Figure 3.11 shows the structural change of ZnO($10\bar{1}0$) under a flow of hydrogen which contains a comparable amount of water as the argon used in the sections above. (A quantification of the water content is presented in Section 3.2.2.) The same roughening process as in argon is observed in Figure 3.11(a) to (c). As can be seen in the flow and pressure curves in Figure 3.12, the roughening begins after 6.4 min of flow when

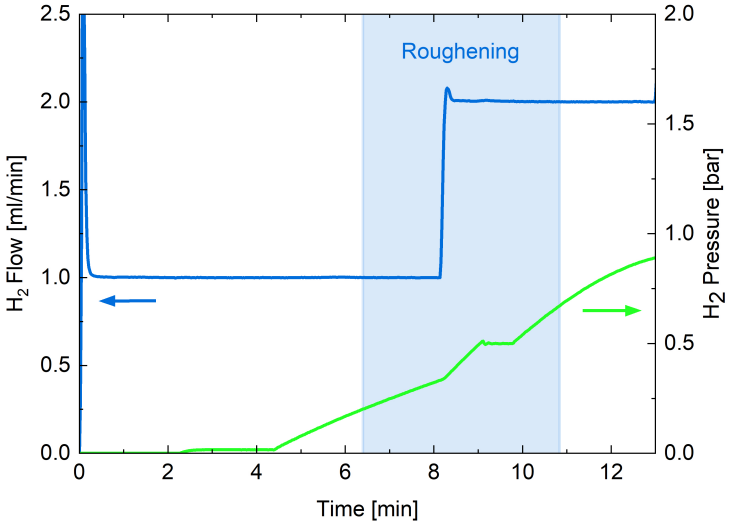

Figure 3.12: Flow and pressure curves of the exposure to up to 1 bar of wet hydrogen. The colored area indicates the roughening of the ZnO as observed in the STM images of which examples are shown in Figure 3.11. The higher peak seen at the beginning of the flow is caused by a pressure build-up that is released when opening the mass flow controller.

the reactor is filled to 0.2 bar of hydrogen. The total amount of gas flown is likely larger than 6.4 ml due to the larger peak of flow during the initial stabilization of the flow. Taking this into account the moment of onset of roughening is in agreement with those observed for water in argon in Section 3.3.4, especially with experiment II. The duration of the roughening process is 4.4 min with a total amount of 7.1 ml of gas. This is comparable to the amount of gas needed in argon in experiment I, although the reactor was filled to a lower pressure when using hydrogen. For this measurement the same sources of inaccuracies as mentioned above (see Section 3.3.4) hold. Overall, the initial roughening in hydrogen environment proceeds in a comparable way as without hydrogen such that we can suggest that the interaction with water proceeds via the same underlying mechanism. It can thus be assumed that ZnO(10$\bar{1}$0) is not covered with hydrogen atoms. The known 1x1 overlayer of H atoms [105] has been calculated to passivate the ZnO(10$\bar{1}$0) surface for adsorption and dissociation of water molecules [113] and would thus prevent the strong interaction with water we see here. This suggests that the nonpolar face does not dissociate hydrogen (to a significant extent) in the 1 bar regime at room temperature. The same has been calculated for UHV conditions where only the polar faces dissociate hydrogen [116]. This could, however, allow for H_2 dissociation at the (0001)- and (000$\bar{1}$)-type step edges of ZnO(10$\bar{1}$0). We do observe

additional structural changes on the ZnO($10\bar{1}0$) surface after the whole terrace has roughened. The size of areas which are not interrupted by steps increases again over time as is visible when comparing Figure 3.11(e) to Figure 3.11(d). As the density of step edges increases during the initial roughening from Figure 3.11(a) to Figure 3.11(c), the dissociation at the polar-type steps could lead to more dissociated hydrogen, which in turn destabilizes the (0001) face [115]. This could lead to the ZnO($10\bar{1}0$) partially flattening out again. However, after more time has passed a larger step density can be observed again as shown in Figure 3.11(f). Overall, this describes a competition of two effects, the formation of steps due to water and the destabilization of these steps due to H_2, which would account for the continued changes in shape. Which of the two processes dominates likely depends on the exact ratio of H_2 and H_2O partial pressures. For technical reasons the surface is exposed to a rough vacuum on the order of 0.1 mbar for a couple of minutes before the flow of hydrogen gas can be initiated. It can thus be assumed that it is saturated with the first monolayer of water at the beginning of the hydrogen exposure, which could explain why the initial roughening is similar to the case without hydrogen.

3.4 Conclusions and Outlook

The use of a ZnO($10\bar{1}0$) single crystal in the ReactorSTM setup is technically feasible but practically challenging for a number of reasons. A preparation procedure using sputtering and annealing which leads to a sufficient cleanliness and flatness has been found. However, extended use in ultra-high vacuum and repeated preparation leads to a loss of conductivity of the crystal and to the incorporation of argon. These limitations are especially challenging for use in high-pressure experiments as intense re-preparation of the sample is usually necessary after exposure to gases in the reactor. The loss of conductivity does not only technically impede STM measurements, but also allows for the formation of large vacancy densities, which can be highly active and strongly influence results. In order to allow for future measurements where repeated preparation is necessary, we recommend a systematic study of hydrogen exposure at elevated temperatures, such that a preparation step which counteracts the loss of conductivity can be incorporated into the preparation procedure. This would allow for more comparable and less time-consuming studies of ZnO($10\bar{1}0$) in the ReactorSTM setup.
We have presented evidence for a significant roughening of the ZnO($10\bar{1}0$) surface in the mbar range of water, which proceeds within the first 10 min and is dependent on the total amount of water supplied to the surface. The formation of different step types during the roughening has been discussed on the basis of their stability in UHV as well as in water background. Preliminary measurements of this roughening in hydro-

gen background suggest that a second process is taking place. Distinguishing the two processes, for example by imaging the surface in dried hydrogen, and understanding their exact balance would be interesting from a fundamental point of view. However, for practical applications the water content in air as well as in industrially used gases is likely higher than in the mbar range, especially during reactions where water is a reactant or product. Thus, it can be assumed that the water content would be high enough for ZnO(10$\bar{1}$0) to be present only in the rough phase at room temperature independent of the hydrogen partial pressure. This limits the applicability of UHV studies on ZnO(10$\bar{1}$0) at room temperature as a model for methanol steam reforming catalysts as well as other ZnO devices. Additionally, the roughening could have influence on the interpretation of data taken at room temperature under elevated water pressures, such as near-ambient pressure XPS, where the surface is not imaged and assumed to be flat ZnO(10$\bar{1}$0). However, in order to evaluate the significance of our findings it is crucial to investigate the influence of temperature on the roughening process. Such an influence is likely, since the interaction of ZnO(10$\bar{1}$0) with the water background in UHV changes when heating up from room temperature to only 400 K (see Section 3.3.1). A study in the range of 500 K surface temperature would be most relevant for catalytic applications.

3.5 Supplemental Information

3.5.1 Preparation and STM of ZnO(10$\bar{1}$0)

A commonly used technique for the preparation of single-crystal surfaces is cycles of argon ion sputtering and annealing in ultra-high vacuum. Additionally, metal samples are frequently annealed in oxygen background in order to react away surface carbon as well as bring other metal impurities to the surface and oxidize them. While there is no concrete evidence as to whether this would be possible or not for oxide samples in general, ZnO(10$\bar{1}$0) is prepared without oxygen annealing in the literature. We have observed a significant increase in the roughness of the sample after oxygen annealing (data not shown), which prevents an estimation of the effect on the cleanliness and requires long annealing in ultra-high vacuum afterwards, thus resulting in an inefficient cleaning process. After increasing the annealing temperature until the crystal became sufficiently flat, the final cleaning recipe was chosen as 20 min sputtering in $1{\cdot}10^{-6}$ mbar of argon with an acceleration voltage of 1.4 kV resulting in a sample current of 4 μA on a surface area of 0.5 cm^2 followed by 20 min of annealing to 795 K in ultra-high vacuum. In the last cycle before imaging the surface the annealing temperature was decreased to 794 K in order to prevent contaminants which are present in the bulk from reaching the surface.

Most STM images shown in this chapter are taken at voltages significantly lower than the bandgap of ZnO at 3.4 eV [117]. Atomic-resolution images of ZnO($10\bar{1}0$) are generally taken at bias voltages of around 2 V or less [105,112,118]. An increase in resolution with decreasing voltage can easily be understood for conductive samples as a lower voltage at constant tunneling current results in the tip moving over the surface at closer proximity. However, the fact that ZnO is sufficiently conductive for scanning tunneling microscopy at all is not entirely understood. For the more commonly used TiO_2 single crystals the conductivity is increased by slightly reducing the material through annealing in ultra-high vacuum, which leads to oxygen vacancies in the surface [119,120]. This method has been proven ineffective for ZnO. A probable cause is that, as density functional theory has shown [121], oxygen vacancies on ZnO($10\bar{1}0$) are unlikely. They might be observed in small coverages only at temperatures above 1000 K and in the absence of O_2 [122]. In comparison, ZnO dimer vacancies show a significantly lower formation energy [121], suggesting that the zinc atom leaves the surface together with the oxygen atom in most cases. Additionally, it has been calculated that, even if present, oxygen vacancies would not contribute to n-type conductivity [123]. There is evidence, however, that hydrogen impurities are donors that contribute to the conductivity of ZnO. These can easily be incorporated during the production of single crystals [123,124].

Although the ZnO($10\bar{1}0$) single crystal was sufficiently conductive for high-resolution imaging in the beginning, we have observed a decrease in scanning resolution with prolonged use of the crystal and repeated preparation in UHV. It was not suitable for high-pressure scanning tunneling microscopy anymore after a total of about 300 cleaning cycles. In order to evaluate the stability of the H impurities contributing to the conductivity it is necessary to distinguish between two different types of impurities, which have been observed and described in detail by Janotti et al. [123] and Shi et al. [124]. The first type of hydrogen impurity, a hydrogen atom bound to a bulk oxygen atom, referred to as OH-type, is only stable up to around 420 K. The second type of hydrogen impurity is a hydrogen atom that replaces an oxygen atom. This so-called substitutional hydrogen is believed to be the main one present in samples which have been cooled down slowly during preparation or stored at room temperature for a long time. It is stable up to higher temperatures of about 770 K. This suggests that repeated preparation of ZnO($10\bar{1}0$) according to the recipe used throughout this work could deplete the sample of the substitutional as well as the OH-type hydrogen, thus decreasing the conductivity. Annealing zinc oxide in ambient pressures of molecular hydrogen to 1000 K can reintroduce hydrogen impurities of both types depending on the cooling process. It is unlikely that this could be done with a single crystal while preserving its structure and flatness. We have observed an improved scanning resolution after ex-

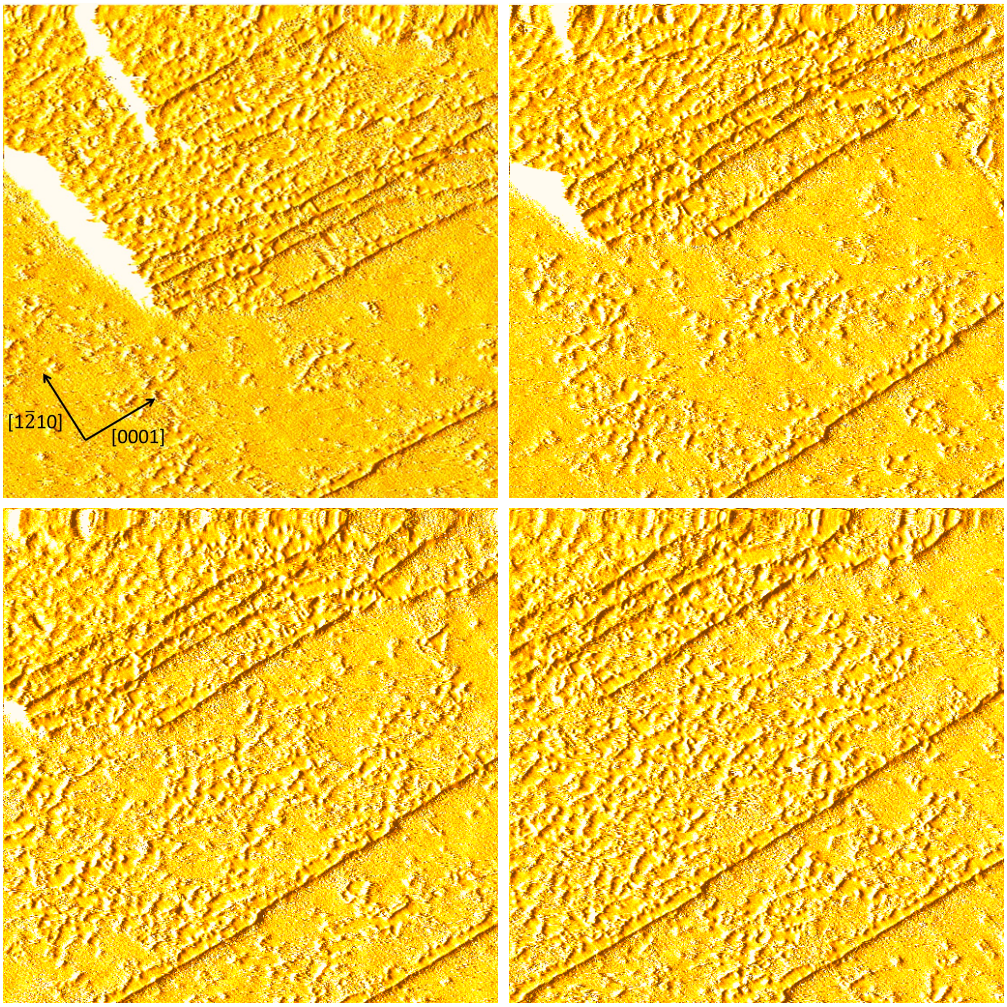

Figure 3.13: Consecutive 80 nm x 80 nm STM images of the as-prepared ZnO(10$\bar{1}$0) surface after roughly 160 cleaning cycles taken at 400 K with + 2.5 V and 50 pA. A derivative of the images is shown here in order to make the pits on all the terraces in the image visible at once.

posure to $1{\cdot}10^{-6}$ mbar of H_2 in the UHV chamber at a surface temperature of 400 K. As the increase in resolution was short-lived, however, it is possible that an adsorption structure of hydrogen or a functionalized tip resulted in sharper images rather than the conductivity of the sample itself recovering. It has been shown that adsorption of atomic hydrogen metallizes the surface [105,107,125]. However, the dissociation of molecular hydrogen has only been observed on the polar faces and not on the $(10\bar{1}0)$ face of ZnO [116]. The effect of low pressures of hydrogen on the resolution has not been investigated systematically here and it is generally difficult to identify one factor alone as the reason for a sudden increase in resolution as there are a large number of factors that play a role in the resolution of an STM. It has been observed previously that prolonged storage in air can recover the conductivity of zinc oxide samples [126]. This is currently the only reliable method we are aware of, although it has not been investigated how and how fast hydrogen can incorporate into zinc oxide in air at room temperature.

3.5.2 Tip-induced Vacancy Formation

Figure 3.13 shows multiple STM images taken in UHV at 400 K on the as-prepared $ZnO(10\bar{1}0)$ surface. The images are taken consecutively at roughly the same position such that the same roughly 30-nm-wide terrace can be identified in all of them. During scanning the density of pits on the terrace increases until it becomes more homogeneously covered with them. The sample drifts to the upper left corner which brings not previously scanned areas with a small vacancy density into the frame from the lower right corner. In additional images (not shown here) the scan size at the same position was increased resulting in the observation of areas of low pit density around the previously scanned area with high density. This is clear evidence that the scanning itself is the cause for the formation of these pits.

A zoom-in of the fourth scan as well as a corresponding height profile can be seen in Figure 3.14. Again a step height of around 0.3 nm is measured (as in Section 3.3.1) while the pits seen on the lower terrace have a depth between 0.1 and 0.15 nm. This is in agreement with one layer of ZnO missing. As the $ZnO(10\bar{1}0)$ step is a double layer of these ZnO dimers, the vacancies are not a step height deep but can have less than half that depth, as has been observed in Ref. [84]. This is illustrated in Figure 3.15.

The larger-resolution image in Figure 3.16 shows that the Zn lines stay intact in between the vacancies. The smallest vacancies, marked with a blue circle, can be identified as a vacancy of one dimer when comparing to simulated STM images based on density functional theory from Ref. [121]. However, most vacancies in this image have already become larger and must consist of several missing dimers. At this stage they can appear longer in parallel or orthogonal direction with respect to the Zn lines. However,

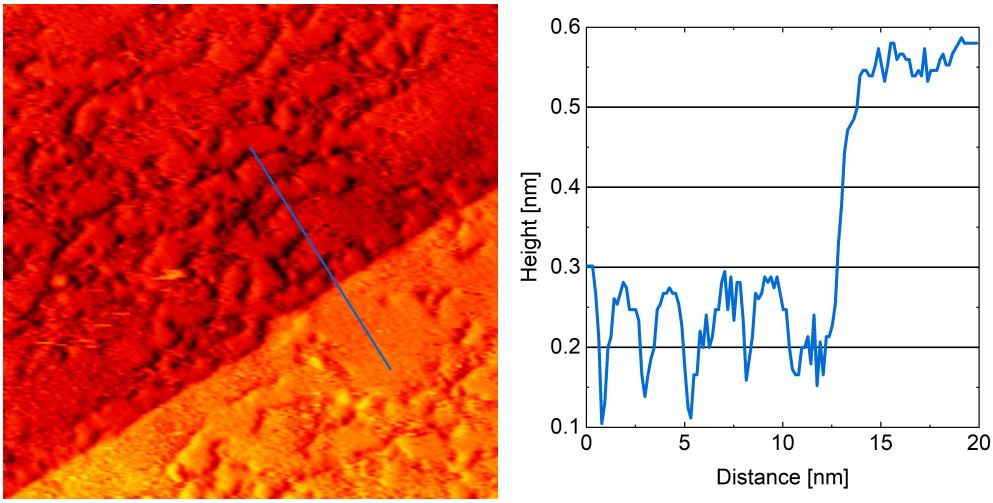

Figure 3.14: 40 nm x 40 nm zoom of the last image in Figure 3.13 with the corresponding height profile indicated in blue. For better visibility of the pits the image is a plane filter merged with its derivative, whereas the height profile is taken at a most common normal plane filter.

during longer scanning, where the vacancies connect to a network as seen in Figures 3.13 and 3.14, they are more often connected in the direction perpendicular to the Zn lines. This suggests that the vacancy growth is favored in the [0001] direction at this stage. As the resolved Zn lines in Figure 3.16 run diagonally from the upper left to the lower right corner of the image, the fast scanning direction of the STM tip (horizontally in all images shown) is at an angle of about 45° with respect to the [0001] as well as the [1$\bar{2}$10] direction. It is thus unlikely that the movement of the tip is the main reason for the preferred direction of the vacancy lines along one direction.

When scanning at bias voltages between 2 V and 3 V, a terrace is covered with vacancies within five to eight scans on the same position. However, when scanning with the same tip speed but bias voltages of 4 V or higher a terrace is already covered with vacancies in the first image taken (data not shown). Although the tip is farther away from the surface, a higher bias voltage also leads to a higher charge on the ZnO surface. The apparent difference between the behavior at 3 V and 4 V could be related to the bandgap of ZnO at 3.4 V [117]. It is thus likely that electronic effects play a role in the removal of the ZnO dimers. However, although the bias voltage is applied to the whole surface, areas without vacancies can be found when moving to an area that was not scanned previously. Thus, the charge alone is not sufficient to create the vacancies. It is rather the (local) tunneling current or a combination of charge effect and mechanical interaction with the tip that is responsible for removing ZnO dimers from the surface.

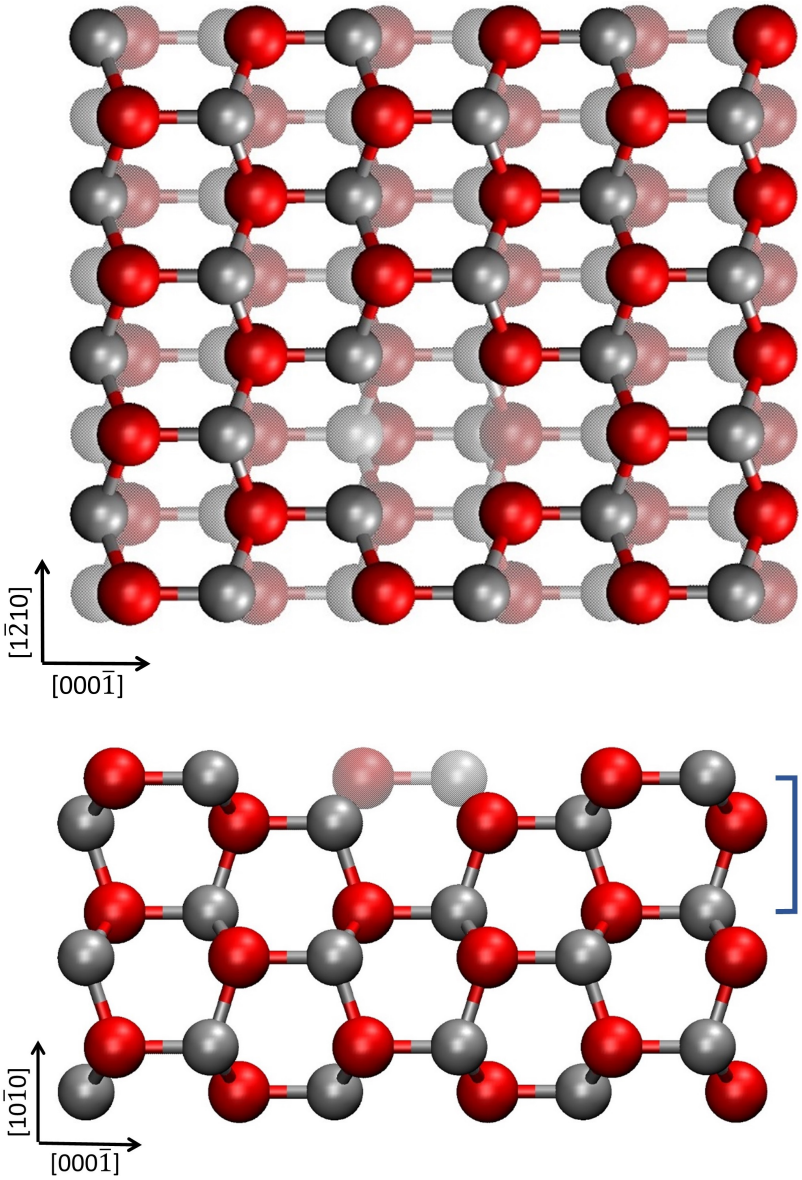

Figure 3.15: Top view (top) and side view (bottom) of a schematic representation of the ZnO(10$\bar{1}$0) surface with one dimer vacancy. Zinc atoms are grey and oxygen atoms red. Atoms in transparent colors are further away from the viewer. The blue line indicates one step height of ZnO(10$\bar{1}$0).

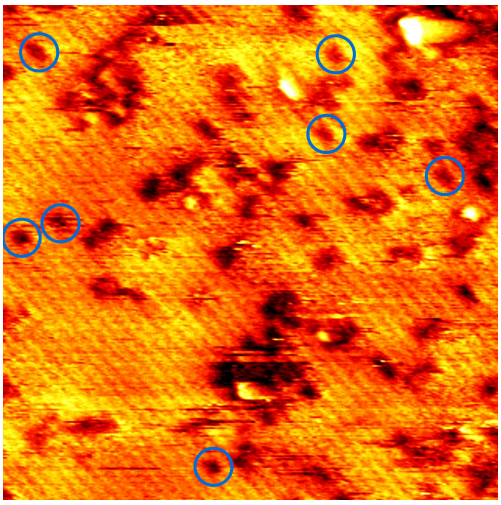

Figure 3.16: 20 nm x 20 nm STM image of ZnO(10$\bar{1}$0) after roughly 160 cleaning cycles taken at 400 K with + 2.5 V and 50 pA. The image has been merged with its derivative for better visibility of the Zn lines.

The same tunneling current and voltages up to 4 V were used in the images in Figures 3.1 and 3.2. Nevertheless, a significantly smaller amount of vacancies is visible in these images, which were taken after less cleaning cycles. In light of the loss of conductivity with repeated preparation described in Section 3.5.1 it is possible that the conductivity was already lower to some extent in the images taken in Figures 3.13 to 3.16, allowing the tip to move closer at all voltages. This suggests that the proximity of the tip is relevant for the vacancy formation and the tunneling current alone is not sufficient. As the mechanism responsible for the conductivity of zinc oxide is not completely understood however, it cannot be excluded that the loss of conductivity is directly related to the underlying electronic effect which enables the vacancy formation. In images taken after even more cleaning cycles, like shown in Sections 3.3.2 and 3.3.4, the formation of vacancies is not observed anymore. These high-pressure scans cannot be directly compared to the scans shown here however, as a number of other processes could be taking place under the influence of gases. Adsorbates can increase the conductivity and thus the tip-sample distance. Additionally, the resolution on the terraces, for example in Figure 3.8(a), is significantly lower, such that a small vacancy density might be present but not visible in the images. Additionally, the roughening observed at these pressures starts as soon as the gas is introduced, diminishing the resolution on the small ZnO(10$\bar{1}$0) patches which are left between the steps.

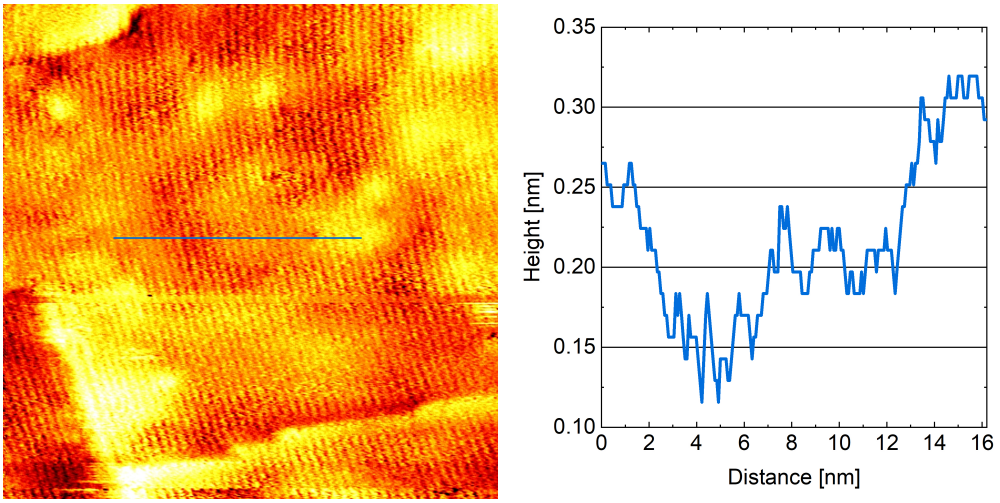

Figure 3.17: 20 nm x 20 nm STM image of the as-prepared ZnO($10\bar{1}0$) surface after more than 300 cleaning cycles taken at 400 K with + 3 V and 50 pA including the corresponding height profile indicated in blue. For better visibility of the Zn lines the image is a plane filter merged with its derivative in a ratio of 2:1, whereas the height profile is taken at a most common normal plane filter.

3.5.3 Incorporation of Argon

In the high-resolution image obtained after about 100 cleaning cycles shown in Figure 3.1(b), brighter and darker areas of about 6 nm diameter can be seen overlaid on the Zn lines. This larger-scale corrugation increases with repeated preparation. It is seen again in Figure 3.16 after about 160 cleaning cycles and more clearly in an image taken after more than 300 cleaning cycles as shown in Figure 3.17. As the Zn lines are not interrupted, the height variances must stem from a subsurface structure. The height profile in Figure 3.17 shows that after more than 300 cleaning cycles the height variation has different levels and is on the order of 0.1 nm. Areas with the same height level can extend up to tens of nanometers. The onset of such a structure is visible in an STM image of ZnO($10\bar{1}0$) in Figure 4(a) in Ref. [118], where it was not investigated further. Shi et al. observe comparable structures on ZnO($10\bar{1}0$) that they identify as subsurface defects [87,89].

It is likely that the height variations observed here are due to the incorporation of argon ions while sputtering during the surface preparation (see Section 3.5.1). Such subsurface ions or so-called argon bubbles have been observed previously with STM on a number of single-crystalline surfaces. Among these are O-ZnO($000\bar{1}$) [118], Co(0001) [127], Ru(0001) [128], Al(111) [129], and PtSi on Si(100) [130]. The last example shows

that argon bubbles can reach diameters of up to the order of a hundred nanometers. This suggests that the dimensions observed here are not unrealistic, although the significantly higher argon acceleration voltage of 20 to 160 kV used in Ref. [130] could facilitate the incorporation and growth of the bubbles. The shape difference between the round argon bubbles observed in the literature on other materials and the network of more irregular height variations in Figure 3.17 could stem from argon bubbles merging over time with increasing incorporation. In comparison to ZnO(10$\bar{1}$0) imaged in Ref. [118], the images presented here are taken after significantly more sputtering and annealing (hundreds instead of tens of cycles), which can explain the more severe height variations observed. Additionally, the higher argon acceleration voltage chosen here (1.4 kV instead of 1 kV in Ref. [118]) could influence the severity and speed of the argon incorporation.

Although the surface layer of the material is not interrupted by argon bubbles, they are known to change the properties of the surface to an extent that can influence its interaction with gases [128,129]. This suggests that argon bubbles have to be taken into account when interpreting measurements on single-crystal model catalysts.

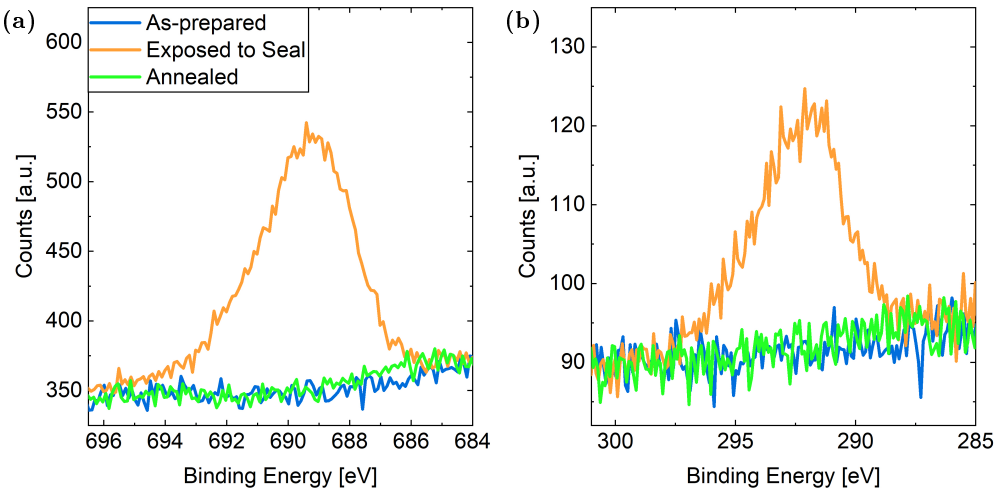

Figure 3.18: (a) F 1s peak and (b) C 1s peak of ZnO(10$\bar{1}$0) taken at room temperature. The as-prepared surface is compared to the same surface after exposure to the reactor seal as well as after an additional annealing step.

3.5.4 Influence of the Reactor Seal

As explained in Section 3.2.1, the reactor is sealed off from the UHV chamber with a Kalrez seal directly on the sample. Although the area of the sample probed by STM is sufficiently far away from the area touched by the seal (on the order of millimeters), residues from the seal need to be removed in order to prevent migration to the probed area. The X-ray photoelectron spectroscope used here probes a lager area of the surface and can thus detect fluorine and carbon residues from the seal. As can be seen in Figure 3.18, no carbon or fluorine is detectable on the as-prepared ZnO($10\bar{1}0$). After exposure to the seal for 3 hours at RT, while keeping the sample in ultra-high vacuum, carbon as well as fluorine are visible in XPS. Annealing the surface to 794 K for one hour removes these residues.
The behavior of the Kalrez seal is temperature-dependent. With increasing temperature the seal between the high-pressure side and the vacuum side generally improves as can be observed in terms of the leak rate into the ultra-high vacuum chamber. Additionally, an elevated temperature facilitates removing the seal from the sample after a high-pressure STM measurement. In order to keep the forces on the sample as small as possible and prevent damage to the specialized oxide sample holder, the seal needs to be removed from the ZnO($10\bar{1}0$) crystal at 400 K surface temperature. This needs to be taken into account when interpreting measurements taken in UHV after removal of the seal including UHV STM, spectroscopy, and diffraction data.